Sensitive quantum state selective detection of H_2O and D_2O by (2+1)-resonance enhanced multiphoton ionization

Gerard Meijer[a] and J. J. ter Meulen
Fysisch Laboratorium, Katholieke Universiteit Nijmegen, Tournooiveld, 6525 ED Nijmegen, The Netherlands

Peter Andresen and Anette Bath
Max-Planck-Institüt fur Strömungsforschung, 4-8 Bottingerstrasse, D-3400 Göttingen, Federal Republic of Germany

(Received 25 July 1986; accepted 25 August 1986)

The first observation of (2 + 1)-REMPI of H_2O and D_2O is reported. With the use of a high power tunable excimer laser radiating at 248 nm, the H_2O and D_2O molecules are ionized after resonant two-photon absorption into the predissociated $\tilde{C}\,^1B_1$ state. The clearly observable peaks in the (2 + 1)-REMPI spectra are all identified and can be used for sensitive state selective detection. Parent molecular fluorescence excitation spectra ($\tilde{C}\,^1B_1 \rightarrow \tilde{A}\,^1B_1$) were remeasured over an increased spectral range, and are remarkably the same as the (2 + 1)-REMPI spectra. Furthermore the OH/OD ($A\,^2\Sigma^+, v' = 0 \rightarrow X\,^2\Pi, v'' = 0$) photofragment fluorescence excitation spectra were measured, and these spectra do not show any nonresonant background as stated before. Additional fluorescence bands starting from the vibrationally excited $A\,^2\Sigma^+, v' = 1$ state were observed. Simulation of the observed REMPI and fluorescence excitation spectra yields the branching ratios for the predissociation, ionization, and fluorescence processes.

I. INTRODUCTION

The photodissociation of H_2O and D_2O via excited Rydberg states, yielding electronically excited OH/OD ($A\,^2\Sigma^+$) photofragments has been the subject of several investigations.[1-3] In the first pioneering studies use has been made of atomic resonance radiation in the VUV. About five years ago Fotakis *et al.*[4] showed that H_2O and D_2O could also be photodissociated via the $\tilde{C}\,^1B_1$ state by the 248 nm radiation of a KrF excimer laser. A large fraction of the $\tilde{C}\,^1B_1 \leftarrow \tilde{X}\,^1A_1$ two-photon absorption band of these molecules lies in the gain profile of this laser. With tunable excimer lasers the photodissociation of H_2O/D_2O via the $\tilde{C}\,^1B_1$ state could be studied more precisely; although the $\tilde{C}\,^1B_1$ state is heavily predissociated there is still enough rotational structure left to allow assignment of rotational quantum numbers in the excited state prior to the dissociation.[5] In Fig. 1 the lowest potential energy curves for H_2O are shown together with the radiative and dissociative processes involving the $\tilde{C}\,^1B_1$ state.

The predissociation mechanism in the $\tilde{C}\,^1B_1$ state of H_2O/D_2O has been first determined by Ashfold *et al.*[6] by means of (3 + 1)-resonance enhanced multiphoton ionization (REMPI) spectroscopy, using a pulsed dye laser around 372 nm. They found a homogeneous, rotation independent, and a heterogeneous, rotation dependent, contribution to the predissociation, only the latter part giving rise to excited OH/OD ($A\,^2\Sigma^+$) photofragments. With the aid of this predissociation mechanism Hodgson *et al.*[5] could explain the observed OH/OD ($A\,^2\Sigma^+ \rightarrow X\,^2\Pi$) photofragment fluorescence excitation spectra following $\tilde{C}\,^1B_1 \leftarrow \tilde{X}\,^1A_1$ two photon absorption in H_2O/D_2O. Recently Docker, Hodgson, and Simons[7] reported the observation of the weak H_2O/D_2O ($\tilde{C}\,^1B_1 \rightarrow \tilde{A}\,^1B_1$) molecular fluorescence excitation spectra around 420 nm from which they could refine the analysis of the heterogeneous predissociation.

In this study the (2 + 1)-REMPI spectra of H_2O/D_2O have been observed for the first time and the photofragment and parent molecular fluorescence excitation spectra have been measured over a larger spectral range than in previous experiments.[5,7] A comparison of all these spectra clearly

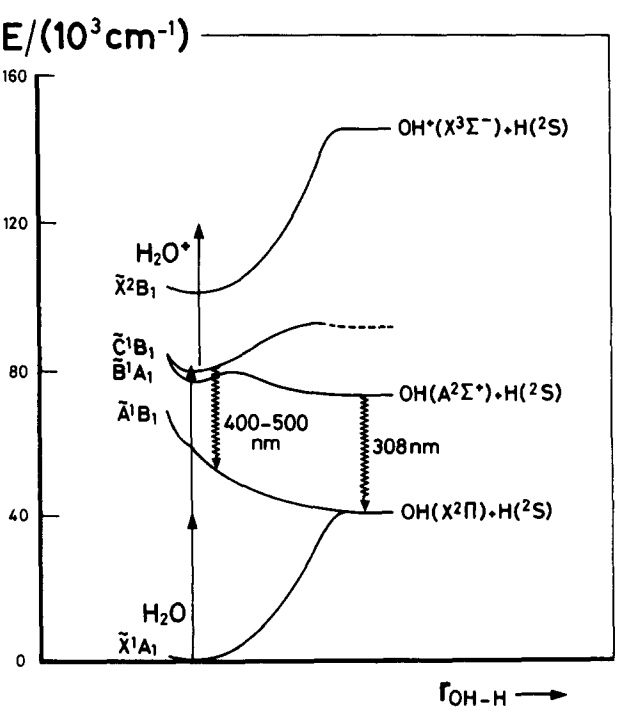

FIG. 1. Correlation diagram showing the processes involved (after Ref. 16).

[a] Guest at MPI, where the experiments were conducted.

 0021-9606/86/246914-09$02.10

shows the state dependent influence of the predissociation, and allows an estimate of the relative importance of the different loss channels (predissociation, fluorescence, and ionization) out of the $\tilde{C}\,^1B_1$ state.

II. EXPERIMENTAL

A schematic view of the experimental setup is given in Fig. 2. The laser radiation was focused through a suprasil entrance window into a stainless steel vacuum chamber where the H_2O or D_2O ($>99.9\%$) was flowing. The radiation source used was an injection locked excimer laser (Lambda Physik EMG 150). This laser system consists of a stable oscillator part, which delivers wavelength selected radiation, and an amplifier part which has unstable optics and is injection locked to the wavelength of the oscillator radiation. The spectral profile of the locked excimer laser consists of a very strong narrow peak at the frequency selected by the oscillator. In addition, however, there is a broadband part with the shape of the gain profile, which can not be totally suppressed. The locking efficiency is defined as the fraction of the total energy that is concentrated in the strong peak.

Line narrowing was achieved in a setup that deviated a little from the commercial one. The end mirror of the oscillator cavity was replaced by a grating reflecting in a high order. In this way less expansion and dispersion prisms could be used in the oscillator cavity while maintaining the same resolution. On the KrF $B \rightarrow X$ transition around 248 nm the laser linewidth was about the same as quoted by the manufacturer ($\sim 0.3\ cm^{-1}$). However, because the losses in the oscillator cavity were lower the oscillator output energy was increased. This improved both the scan range ($\sim 150\ cm^{-1}$) and the locking efficiency of the laser, the latter being very important as will be seen in the discussion of the remeasured OH/OD ($A \rightarrow X$) photofragment fluorescence excitation spectra. If on the other hand the original number of prisms is used in the oscillator cavity, replacement of the end mirror by the grating gives a reduction of the laser linewidth. With the laser system operating on ArF (193 nm) the laser linewidth could be reduced in this way from ~ 3 to $\sim 0.5\ cm^{-1}$. The total scan range and locking efficiency were now almost unaltered. The laser linewidth was measured indirectly in this case by recording the (2 + 1)-REMPI spectrum of H_2.[8] Several two-photon transitions starting from the lowest rotational levels in the $X\,^1\Sigma_g^+$, $v'' = 0$ ground state of H_2 to the excited $E,F\,^1\Sigma_g^+$, $v' = 2$ state lie in the gain profile of the ArF excimer laser, and very strong (2 + 1)-REMPI spectra can easily be observed. The width of the ion peaks in these spectra is determined by the effective two-photon absorption laser linewidth. So if a Lorentzian spectral profile is assumed for the locked part of the laser radiation the laser linewidth is half the width of the ion peaks.

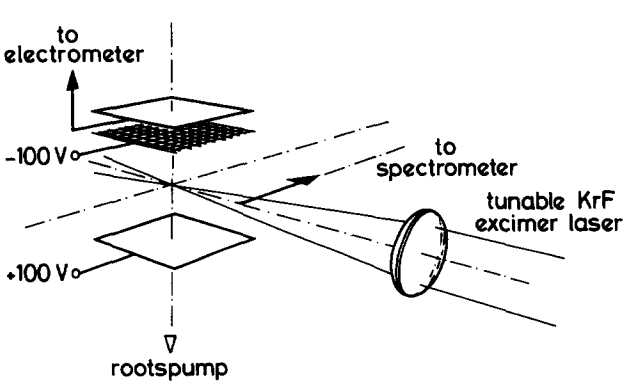

FIG. 2. Schematic overview of the experimental setup. The arrow indicates that fluorescence is essentially sampled a few cm away from the beam waist.

The laser wavelength was scanned with a stepper motor, vibration free, attached to a micrometer screw changing the angle of incidence on the grating.

For the ion detection two copper disks, about 2 cm in diameter and 3 cm apart with a small-mesh grid just in front of one of them were mounted insulated from each other. The laser beam was focused between the disks where an electric field was applied such that positive ions were detected on the unbiased plate, after having passed the grid. Several lenses with different focal lengths between 10 and 100 cm have been used to focus the laser beam. Most data were taken with a 20 cm lens. The strength of the applied electric field in the detection region was not critical. At values of E between 50 and 100 V/cm the best results were obtained. The (2 + 1)-REMPI spectra were recorded at relatively low gas pressures, 5–50 mTorr, in the region around the focus of the excimer laser beam.

In order to suppress the nonresonant ion yield, which had a cubic or even higher dependence on the applied laser power, it turned out to be advantageous to lower the energy of the incoming laser pulse to about 50–100 mJ by placing attenuators (wire nettings) in the laser beam. As shown in Fig. 3 the resonant ion signals had a power dependence varying from nearly quadratic for H_2O to nearly cubic for D_2O at the energies employed. Consequently attenuation of the laser beam caused a stronger reduction of the nonresonant background and the spectra had better contrast this way. The remaining ion signals were still large enough to be detected with a dc electrometer (Rhode & Schwartz UIG-BN12062). At resonance the ion signal was typically several tenths of a nA (dc). At a repetition rate of 8 Hz this implies that a few times 10^8 ions are detected per quantum state per laser pulse.

Total undispersed fluorescence radiation both from the photofragment and from its parent molecule was detected in a direction perpendicular to the incident laser beam using a cooled photomultiplier tube (RCA 31034). The PMT was placed behing a 0.3 m spectrometer (McPherson 218), with its slits completely opened, thus acting as a bandpass filter with a half-width of ~ 4 nm. The optimum H_2O/D_2O pressure for the OH/OD photofragment fluorescence was between 50 and 500 mTorr, whereas the intensity of the H_2O/D_2O molecular fluorescence increased almost linearly with pressure and could be seen the best at the highest possible pressure (15–20 Torr). In both cases the viewed region was a few cm away from the laser beam waist created by a lens with a focal length of typically 25 or 50 cm. At that position the fluorescence signals were maximum and no effect of line broadening due to competing ionization was seen,

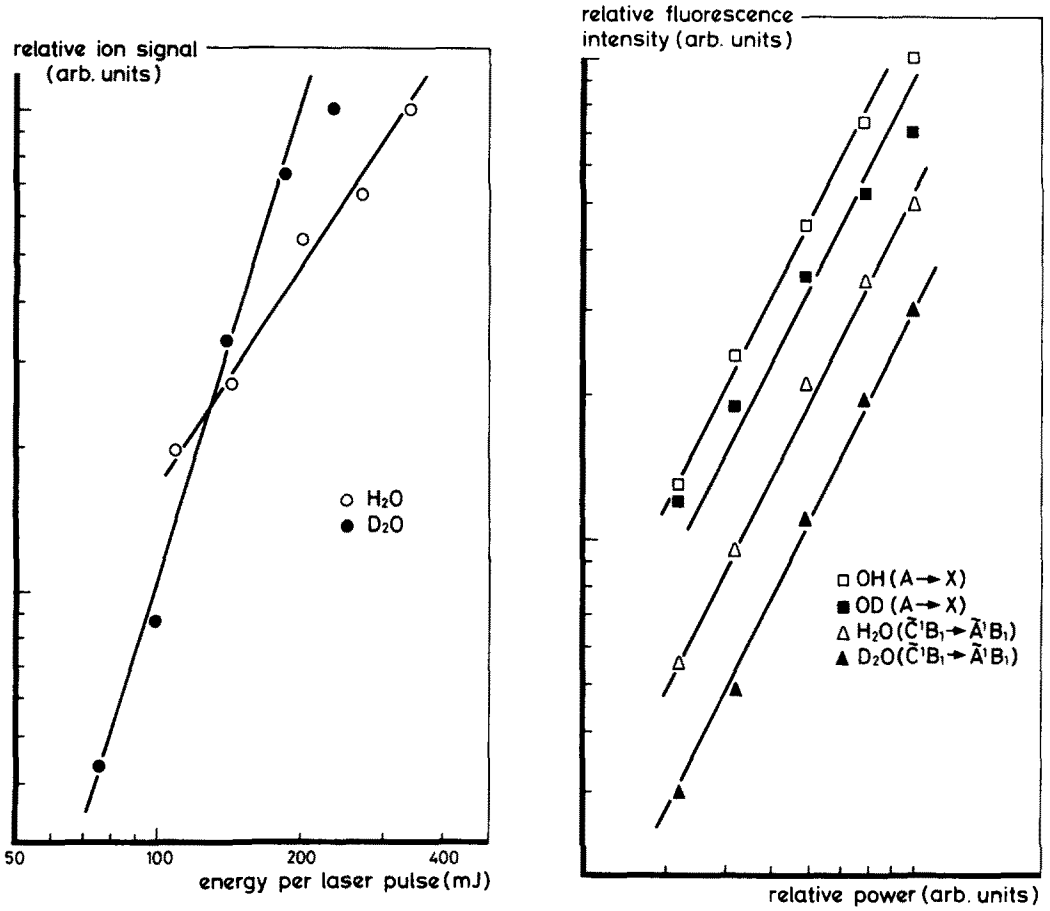

FIG. 3. Power dependence of the ion and fluorescence signals in log–log plots. At least three different excitation wavelengths, yielding the strongest signals, were employed with the same result in all cases. The ions were produced in the focus of a 20 cm lens. Power dependencies equal to $P^{3/2}$ for H_2O and to P^3 for D_2O are indicated in the ion plots. Fluorescence was viewed away from the focus. In these plots a quadratic behavior is indicated to guide the eye.

although even here the power density was about 0.1 GW/cm^2. The fluorescence signals had a quadratic dependence on the applied laser energy (Fig. 3), so the two-photon absorption step was not yet saturated.

In most cases fluorescence and REMPI spectra were recorded separately because laser light scattering from the copper disks lead to a higher radiation background. In the few cases that these spectra were recorded simultaneously and fluorescence was viewed from the region near the focus, a broadening could be observed of the fluorescence spectral lines from those excited levels that also gave rise to strong REMPI peaks.

III. RESULTS AND DISCUSSION

A. OH/OD photofragment fluorescence excitation spectra

The total undispersed OH and OD photofragment ($A \rightarrow X$) fluorescence excitation spectra generated via two-photon absorption into the $\tilde{C}\,^1B_1$ state are shown in Figs. 4 and 5, respectively. These spectra were first observed by Hodgson *et al.*[5] who were able to explain the observed structure quantitatively as being due to two-photon transitions to heavily predissociated rotational levels in the excited state. For this interpretation the two-photon transition probabilities as calculated by Dixon[9] were used as well as the predissociation rates known from the (3 + 1)-REMPI spectra of H_2O/D_2O.[6]

First we observed spectra which were identical to those measured before[5] including the large nonresonant fluorescence background. We found that this was due to poor locking of the laser, even with the end mirror replaced by the

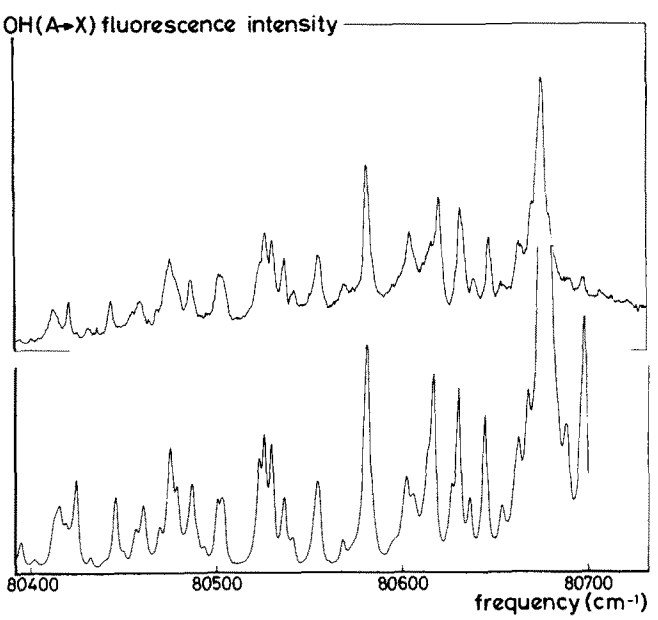

FIG. 4. Observed (upper) and simulated (lower) total undispersed OH ($A \rightarrow X$) fluorescence excitation spectrum.

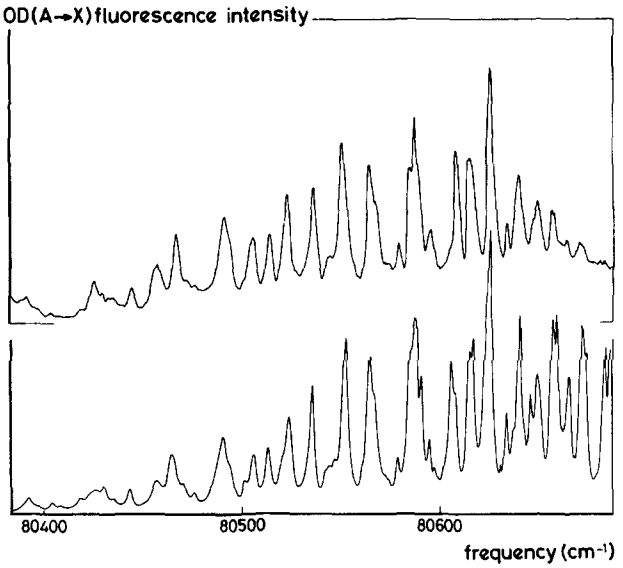

FIG. 5. Observed (upper) and simulated (lower) total undispersed OD ($A \rightarrow X$) fluorescence excitation spectrum.

grating. The locking could be improved by optimizing the OH ($A \rightarrow X$) fluorescence signal on the strong peak at the high frequency side of the spectrum (Fig. 4). This peak can hardly be seen with a poorly locked laser and is therefore perfectly suited for optimization. In fact the locking efficiency is improved by a slight misadjustment of the amplifier optics which decreases the intensity of the broadband part of the laser profile. With the laser locked this way the nonresonant fluorescence background completely disappeared.

Hodgson *et al.*[5] attributed this fluorescence background to direct two-photon absorption into the dissociative $\tilde{B}\,^1A_1$ state. This is obviously not true because the fluorescence background disappears when the laser is better locked. We believe that this fluorescence background is due to the absorption of one photon from the locked and one photon from the unlocked (broadband) part of the laser pulse into the $\tilde{C}\,^1B_1$ state. It can be shown that in this case the spectral profile of the fluorescence background should resemble the gain profile of the laser, as is observed indeed. The most important reason for Hodgson *et al.*[5] to attribute the fluorescence background to another electronic transition ($^1A_1 \leftarrow {}^1A_1$) came from alignment measurements. They used linearly polarized radiation produced by placing a polarizer in the oscillator cavity and measured the alignment $A_0^{(2)}$ of the OH/OD $A\,^2\Sigma^+$ photofragments. It was found that this alignment was larger than the theoretical maximum ($A_0^{(2)} = 2/7$) for a $B_1 \leftarrow A_1$ two-photon transition when the excimer laser was centered on a position where the contribution of the fluorescence background was relatively large. The alignment even reached a maximum value of $A_0^{(2)} \sim 0.6$ when the photofragments were formed without resonant absorption at all. Because according to the theory outlined by Loge and Wiesenfeld[10] an $A_1 \leftarrow A_1$ two-photon transition gives a larger value for the theoretical maximum $A_0^{(2)} = 8/7$, they assumed that a large part of the background was due to the $\tilde{B}\,^1A_1 \leftarrow \tilde{X}\,^1A_1$ two-photon transition. It should be noted, however, that also a $B_1 \leftarrow A_1$ two-photon transition induced by one linearly polarized photon from the locked and one unpolarized photon from the broadband part of the laser pulse can explain this larger value of the alignment. If the formulas of Loge and Wiesenfeld[10] are used a maximum value of $A_0^{(2)} = 7/11$ is found for this case, which agrees very well with the maximum value observed by Hodgson *et al.*[5]

The spectra of Figs. 4 and 5 can be simulated when two different types of predissociation are assumed. First a homogeneous rotation independent predissociation ending up in a dark state, and second a heterogeneous predissociation into the dissociative $\tilde{B}\,^1A_1$ state. The latter predissociation is symmetry allowed only if there is rotation along the a axis, so if $\langle J_a'^2 \rangle > 0$, and via this pathway the observed excited photofragments are formed.[5,6] The simulated spectra are shown below the observed spectra in the same figures. In comparing the simulated and observed spectra the falloff in locking efficiency of the laser below 80 400 cm^{-1} and above 80 640 cm^{-1} should be taken into account. The exact simulation procedure we followed is discussed in Sec. III D.

Besides the well known OH/OD ($A\,^2\Sigma^+, v' = 0 \rightarrow X\,^2\Pi, v'' = 0$) fluorescence around 308 nm, we also observed an order of magnitude less intense fluorescence bands around 285 nm in photodissociating H_2O and around 290 and 335 nm in photodissociating D_2O. These bands were observed under the same experimental conditions as the fluorescence around 308 nm. The excitation spectra of these fluorescence bands were even into the smallest detail identical to the photofragment fluorescence excitation spectra shown in Figs. 4 and 5 and are therefore not shown here. Also the total fluorescence intensity of these bands had a quadratic laser power dependence. Although single fluorescence lines could not be resolved in the present setup, this, together with the position and shape of the bands,[12] seems to justify the identification of the bands around 285/290 nm as being OH/OD ($A\,^2\Sigma^+, v' = 1 \rightarrow X\,^2\Pi, v'' = 0$) fluorescence. This means that in the photodissociation of H_2O/D_2O via the $\tilde{C}\,^1B_1$ state OH/OD ($A\,^2\Sigma^+$) photofragments are partially formed vibrationally hot. The observed ratio for the integrated intensity of the fluorescence from $A\,^2\Sigma^+, v' = 1$ to that from $A\,^2\Sigma^+, v' = 0$ is ~ 0.05 for H_2O and ~ 0.03 for D_2O. Taking the Einstein transition probabilities and electronic transition wave numbers from Refs. 13 and 14 we conclude that about 15% of the OH ($A\,^2\Sigma^+$) and about 10% of the OD ($A\,^2\Sigma^+$) photofragments is formed in the $v' = 1$ state. Hodgson *et al.*[5] did not observe vibrationally excited photofragments in their experiment. However, from experiments in which H_2O is photodissociated with the Lyman-α resonance line of hydrogen at 121.6 nm[1] or with Kr resonance radiation at 123.6 nm,[2] most probably ending up in the $\tilde{D}\,^1A_1$ and the $\tilde{B}\,^1A_1$ state of the parent molecule,[3] respectively, it is known that almost 30% of the OH ($A\,^2\Sigma^+$) molecules are formed in the $v' = 1$ state. In photodissociating via the $\tilde{C}\,^1B_1$ state we now find a somewhat smaller value.

The extra fluorescence band around 335 nm, observed in the photodissociation of D_2O, has about the same integrated intensity as the band around 290 nm and might be attributed to the OD ($A\,^2\Sigma^+, v' = 0 \rightarrow X\,^2\Pi, v'' = 1$) transition. This band however is at least a factor of 10 more intense as should be expected from the published Franck–Condon

factors.[17] Furthermore, the corresponding band in OH around 344 nm, expected to be equally strong, could not be detected which makes the assignment doubtful.

B. (2+1)-REMPI spectra of H_2O and D_2O

In order to obtain the (2 + 1)-REMPI spectra of H_2O and D_2O optimal locking of the laser system is very important. With a poorly locked laser only a broad structureless ion spectrum with no resonances at all, resembling the gain profile of the laser, is observed. As in the case of the fluorescence spectra this must be attributed to a smearing out of rotational structure by the absorption of photons both from the locked and the unlocked part of the laser pulse.

In Figs. 6 and 7 the observed (2 + 1)-REMPI spectra of H_2O and D_2O are shown. If it is assumed that the third ionizing photon does not influence the spectral structure, i.e., if the overall MPI transition probability is governed by the initial two-photon absorption event, direct spectroscopic information about the excited $\tilde{C}\,^1B_1$ state can be obtained from these spectra. As expected these spectra reflect the already described predissociation mechanism. The strongest signals arise from levels that are least predissociated, which are levels with a low value of $\langle J_a'^2 \rangle$. Therefore the (2 + 1)-REMPI spectra are completely different from the photofragment fluorescence excitation spectra. Furthermore it is readily seen that the (2 + 1)-REMPI spectra consist of somewhat broader lines than the fluorescence spectra. This broadening cannot be explained by overlapping rotational features, and is most probably due to the extra ionization loss channel out of the excited $\tilde{C}\,^1B_1$ state which is present when the power density is as high as employed in the region of ion production (we estimate roughly $\sim 10\,\mathrm{GW/cm^2}$). The ionization loss channel reduces the lifetime of the rotational levels in the $\tilde{C}\,^1B_1$ state, giving rise to an extra line broadening and a decrease in peak intensity. In this way both peak heights and linewidths in the (2 + 1)-REMPI spectra can be fairly well simulated. There may be a small additional effect from power broadening, especially for H_2O where the $P^{3/2}$ power dependence expected for spatial saturation[15] is approached (Fig. 3).

In Tables I and II the two-photon transitions having the largest contributions to the different peaks in the (2 + 1)-REMPI spectra are tabulated, including their calculated relative intensities (see Sec. III D). The numbering of the lines corresponds to the numbering in Figs. 6 and 7 of the observed (2 + 1)-REMPI spectra.

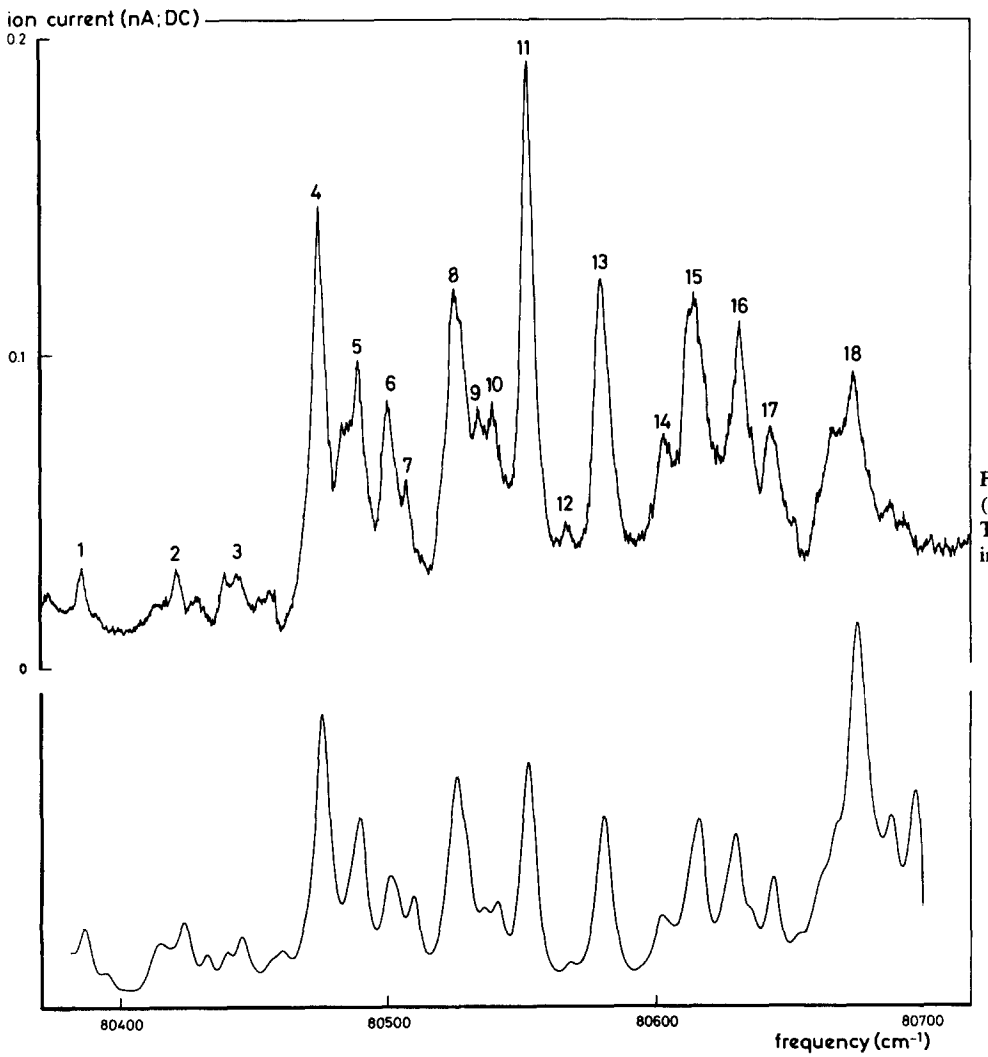

FIG. 6. Observed (upper) and simulated (lower) (2 + 1)-REMPI spectrum of H_2O. The line numbers are related to the numbers in Table I.

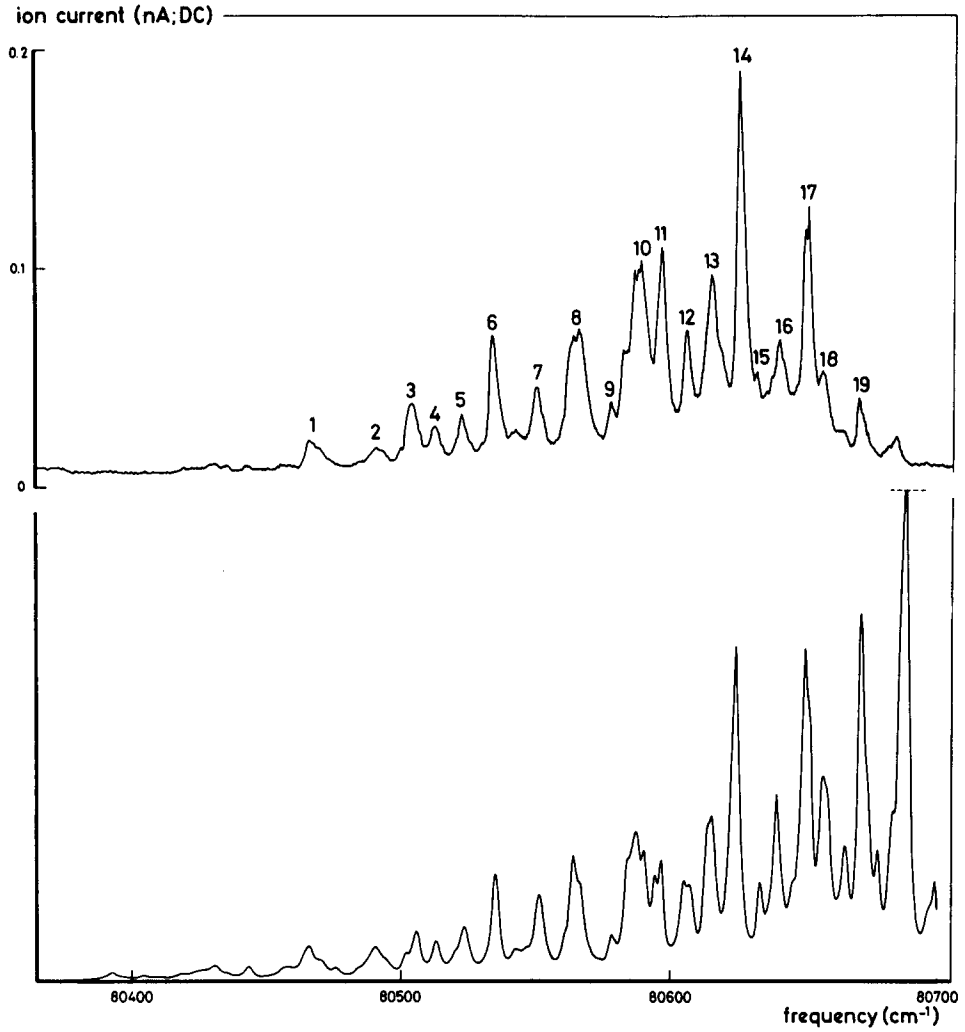

FIG. 7. Observed (upper) and simulated (lower) (2 + 1)-REMPI spectrum of D_2O. The line numbers are related to the numbers in Table II.

C. The H_2O/D_2O molecular fluorescence excitation spectra

Recently Docker *et al.*[7] reported the bound free emission in H_2O/D_2O from rotational levels in the $\tilde{C}\ ^1B_1$ state to the dissociative $\tilde{A}\ ^1B_1$ state, around 400–500 nm. The quantum yield for this fluorescence[7] is small, $\sim 10^{-4}$, but it can be seen fairly strong at high gas pressures. The lifetime of the upper state is fully determined by the fast predissociation and even at the highest pressures used (15–20 Torr) no effects of quenching have been observed and the fluorescence intensity increases linearly with pressure.

This blue fluorescence is most intense from those excited levels that are least predissociated. Consequently the molecular fluorescence excitation spectra of H_2O/D_2O are expected to have more or less the same shape as the (2 + 1)-REMPI spectra. Indeed, we observed that these two types of spectra, although recorded under different experimental conditions, are remarkably similar. The only difference between the observed molecular fluorescence excitation spectra, shown in Figs. 8 and 9, and the (2 + 1)-REMPI spectra is the smaller linewidth of the former spectra due to the much lower power density in the fluorescence detection region than in the region of ion production.

The resemblance between the (2 + 1)-REMPI spectra and the molecular fluorescence excitation spectra indicates explicitly that the structure observed in the (2 + 1)-REMPI spectra is determined by the two-photon absorption process and is hardly influenced by the third ionizing photon. Furthermore, small differences between the two spectra can indicate a possible resonance enhancement in the absorption of the third photon. For example, peak no. 11 in the (2 + 1)-REMPI spectrum of H_2O is about 50% stronger than expected from the simulation, while on the other hand, the corresponding peak in the H_2O ($\tilde{C}\ ^1B_1 \rightarrow \tilde{A}\ ^1B_1$) fluorescence excitation spectrum does behave as expected. Because it is only one peak that shows up too strong it is quite unlikely that this is due to saturation in the REMPI spectrum.

D. Simulation of the spectra

For the simulation of the spectra the relative two-photon absorption line strengths (h_0) and absorption frequencies as calculated by Dixon[9] were used. The line strengths include an assumed Boltzmann distribution in the ground state with a rotational temperature $T_r = 300$ K.

TABLE I. Calculated two-photon absorption frequencies (Ref. 9) and ion signal intensities for the (2 + 1)-REMPI spectrum of H_2O. Only the transitions that contribute strongest to the different peaks are given. The line numbers refer to Fig. 6.

Line no.	ν/cm^{-1}	Transition $\tilde{C}\,^1B_1 \leftarrow \tilde{X}\,^1A_1$	Relative intensity
1	80 387.1	$2_{02} \leftarrow 4_{23}$	3.20
2	80 424.3	$2_{11} \leftarrow 3_{30}$	3.52
3	80 445.2	$6_{06} \leftarrow 7_{07}$	2.01
	80 445.9	$6_{16} \leftarrow 7_{17}$	0.65
4	80 474.9	$5_{15} \leftarrow 6_{16}$	3.05
	80 475.3	$2_{02} \leftarrow 3_{21}$	10.00
5	80 486.8	$4_{13} \leftarrow 4_{32}$	2.25
	80 489.8	$0_{00} \leftarrow 2_{21}$	6.63
6	80 500.3	$4_{04} \leftarrow 5_{05}$	3.84
	80 502.8	$4_{14} \leftarrow 5_{15}$	1.36
	80 504.2	$5_{05} \leftarrow 5_{24}$	1.48
7	80 509.7	$1_{01} \leftarrow 2_{20}$	4.31
8	80 523.0	$5_{15} \leftarrow 5_{14}$	3.34
	80 525.4	$4_{04} \leftarrow 4_{23}$	7.35
	80 529.5	$3_{13} \leftarrow 4_{14}$	4.64
9	80 536.4	$2_{11} \leftarrow 3_{12}$	2.46
10	80 541.6	$3_{03} \leftarrow 3_{22}$	3.29
11	80 552.5	$2_{02} \leftarrow 2_{21}$	9.24
12	80 568.1	$1_{10} \leftarrow 2_{11}$	1.03
13	80 579.6	$1_{11} \leftarrow 2_{12}$	3.33
	80 581.0	$3_{13} \leftarrow 3_{12}$	6.08
14	80 602.3	$2_{12} \leftarrow 2_{11}$	2.20
15	80 613.6	$4_{04} \leftarrow 3_{21}$	2.24
	80 616.8	$1_{11} \leftarrow 1_{10}$	7.16
16	80 626.1	$1_{10} \leftarrow 1_{11}$	2.45
	80 630.1	$2_{11} \leftarrow 2_{12}$	7.13
17	80 644.3	$4_{13} \leftarrow 4_{14}$	5.58
18	80 674.8	$3_{13} \leftarrow 2_{12}$	5.73
	80 675.0	$5_{24} \leftarrow 5_{05}$	3.16
	80 675.9	$3_{22} \leftarrow 3_{03}$	5.81

TABLE II. Calculated two-photon absorption frequencies (Ref. 9) and ion signal intensities for the (2 + 1)-REMPI spectrum of D_2O. Only the transitions that contribute strongest to the different peaks are given. The line numbers refer to Fig. 7.

Line no.	ν/cm^{-1}	Transition $\tilde{C}\,^1B_1 \leftarrow \tilde{X}\,^1A_1$	Relative intensity
1	80 465.5	$5_{23} \leftarrow 7_{44}$	0.25
	80 466.4	$7_{07} \leftarrow 9_{28}$	0.39
2	80 488.6	$3_{30} \leftarrow 5_{51}$	0.22
	80 490.9	$4_{23} \leftarrow 6_{42}$	0.34
3	80 505.5	$6_{16} \leftarrow 8_{17}$	0.51
	80 506.6	$5_{14} \leftarrow 7_{35}$	0.69
4	80 513.1	$4_{14} \leftarrow 6_{33}$	0.48
	80 513.8	$7_{25} \leftarrow 8_{44}$	0.37
5	80 522.6	$3_{22} \leftarrow 5_{41}$	0.28
	80 523.6	$7_{07} \leftarrow 8_{26}$	0.45
	80 524.1	$3_{21} \leftarrow 5_{42}$	0.58
6	80 535.2	$5_{05} \leftarrow 7_{26}$	1.17
	80 535.8	$4_{13} \leftarrow 6_{34}$	0.53
	80 535.8	$7_{16} \leftarrow 8_{35}$	0.68
	80 536.2	$6_{16} \leftarrow 7_{35}$	0.67
7	80 551.0	$3_{13} \leftarrow 5_{32}$	0.47
	80 552.0	$5_{23} \leftarrow 6_{42}$	0.59
	80 552.2	$2_{21} \leftarrow 4_{40}$	0.91
	80 552.5	$2_{20} \leftarrow 4_{41}$	0.46
8	80 563.7	$3_{12} \leftarrow 5_{33}$	1.48
	80 564.5	$6_{15} \leftarrow 7_{34}$	0.70
	80 565.1	$5_{15} \leftarrow 6_{34}$	0.56
	80 565.3	$4_{23} \leftarrow 5_{42}$	0.56
9	80 584.5	$2_{12} \leftarrow 4_{31}$	1.64
10	80 588.4	$5_{14} \leftarrow 6_{33}$	2.28
	80 590.6	$2_{11} \leftarrow 4_{32}$	1.01
	80 591.1	$4_{14} \leftarrow 5_{33}$	1.68
11	80 595.2	$5_{05} \leftarrow 6_{24}$	2.11
	80 597.4	$3_{03} \leftarrow 5_{24}$	2.76
12	80 605.7	$9_{09} \leftarrow 10_{010}$	1.09
	80 605.8	$9_{19} \leftarrow 10_{110}$	0.53
	80 608.2	$4_{13} \leftarrow 5_{32}$	1.48
13	80 614.1	$3_{13} \leftarrow 4_{32}$	1.09
	80 614.6	$1_{11} \leftarrow 3_{30}$	1.38
	80 616.5	$1_{10} \leftarrow 3_{31}$	2.95
14	80 623.8	$8_{18} \leftarrow 9_{19}$	1.59
	80 625.0	$3_{12} \leftarrow 4_{31}$	3.16
	80 625.3	$9_{09} \leftarrow 9_{28}$	2.11
	80 625.8	$2_{02} \leftarrow 4_{23}$	1.79
15	80 634.2	$2_{12} \leftarrow 3_{31}$	2.18
16	80 639.8	$2_{11} \leftarrow 3_{30}$	1.33
	80 640.6	$7_{07} \leftarrow 8_{08}$	2.37
	80 641.0	$7_{17} \leftarrow 8_{18}$	1.11
17	80 650.8	$3_{03} \leftarrow 4_{22}$	7.15
	80 652.7	$1_{01} \leftarrow 3_{22}$	4.26
18	80 656.7	$6_{06} \leftarrow 7_{07}$	1.56
	80 657.4	$6_{16} \leftarrow 7_{17}$	2.82
	80 659.4	$7_{07} \leftarrow 7_{26}$	2.55
19	80 671.7	$2_{02} \leftarrow 3_{21}$	4.77
	80 671.9	$5_{05} \leftarrow 6_{06}$	3.61
	80 673.1	$5_{15} \leftarrow 6_{16}$	1.63
	80 674.2	$6_{06} \leftarrow 6_{25}$	2.01

The observed linewidth in the measured spectra is almost completely determined by the short lifetime of the upper state. Homogeneous predissociation out of the $\tilde{C}\,^1B_1$ state causes a Lorentzian line shape with a linewidth $\Delta\nu_0$. The heterogeneous predissociation gives an extra term to this linewidth which can be represented by $\Delta\nu_0 c\langle J_a'^2\rangle$, using the same model as used by Ashfold *et al.*[6] The parameter c is a measure of the relative importance of the heterogeneous predissociation with respect to the homogeneous predissociation. Values of $\langle J_a'^2\rangle$ are calculated using the rotational constants as given by Johns.[11] For ease of computation the laser line shape was chosen to be Lorentzian with a linewidth of $\sim$0.6 cm^{-1}, twice the linewidth at the fundamental frequency. Although the linewidth is important for the value of $\Delta\nu_0$, the exact form of the laser profile was not critical.

For the two-photon absorption process the relative peak heights h_{ab} and linewidths $\Delta\nu$ of the different transitions are calculated according to

$$\Delta\nu = (1 + c\langle J_a'^2\rangle + \beta)\cdot\Delta\nu_0,$$
$$h_{ab} = h_0/(1 + c\langle J_a'^2\rangle + \beta). \quad (1)$$

In these formulas the term β takes other loss channels that reduce the lifetime of the $\tilde{C}\,^1B_1$ state into account, e.g., fluorescence and ionization.

First we fitted the homogeneous half-width $\Delta\nu_0$ and the parameter c by simulating the H_2O/D_2O ($\tilde{C}\,^1B_1 \rightarrow \tilde{A}\,^1B_1$) fluorescence excitation spectra. These spectra were recorded in a region with a relatively low power density so the ionization rate could be neglected compared to the predissociation

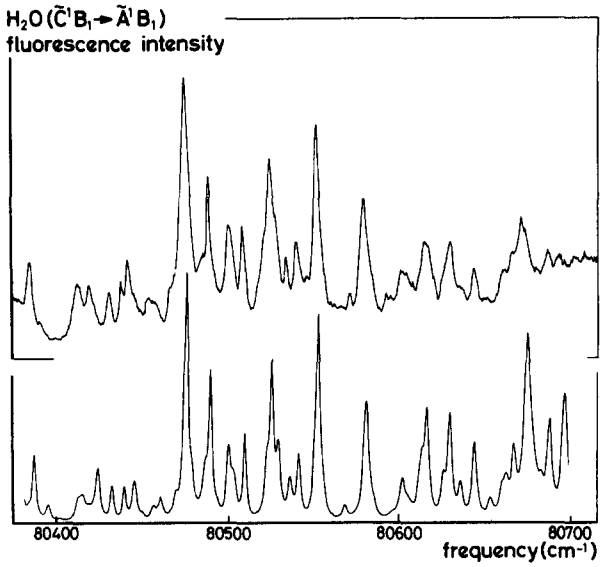

FIG. 8. Observed (upper) and simulated (lower) total undispersed ($\tilde{C}\,^1B_1 \rightarrow \tilde{A}\,^1B_1$) excitation spectrum of H_2O.

rate. There is a contribution to β from the $\tilde{C}\,^1B_1 \rightarrow \tilde{A}\,^1B_1$ fluorescence. However, the fraction of excited molecules that fluoresces is equal to $\beta/(1+c\langle J_a'^2\rangle+\beta)$ which is about 10^{-4}. Consequently the term β can be neglected compared with the predissociation in the expressions (1), and in the simulation of the fluorescence spectra the following formulas are used:

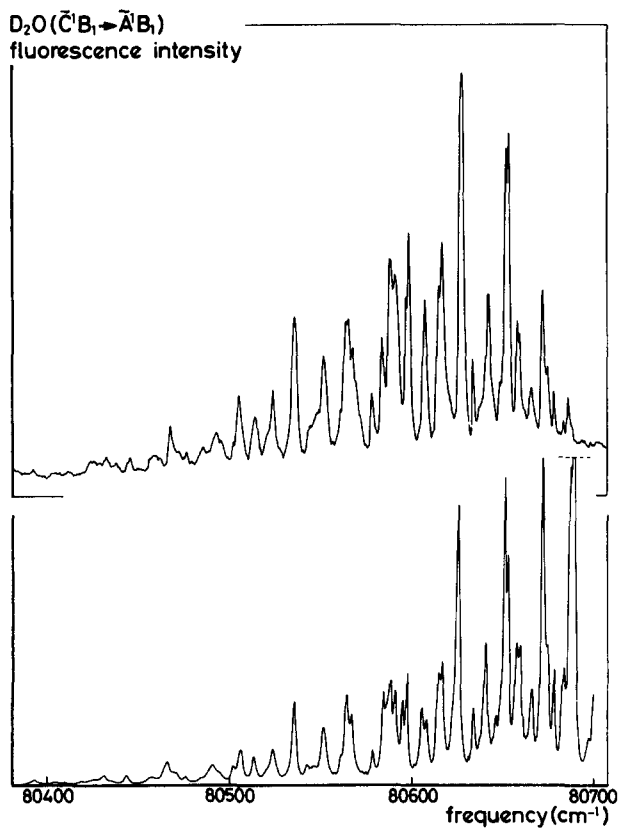

FIG. 9. Observed (upper) and simulated (lower) total undispersed ($\tilde{C}\,^1B_1 \rightarrow \tilde{A}\,^1B_1$) excitation spectrum of D_2O.

$$\Delta\nu = (1+c\langle J_a'^2\rangle)\cdot\Delta\nu_0,$$
$$h_{\text{fl}}(:)h_0/(1+c\langle J_a'^2\rangle)^2. \tag{2}$$

Very good agreement between calculated and observed spectra was obtained for a homogeneous predissociation rate $k_p = 4\times10^{11}$ s^{-1} ($\Delta\nu_0 = 2.1$ cm^{-1}) for H_2O and $k_p = 1.9\times10^{11}$ s^{-1} ($\Delta\nu_0 = 1.0$ cm^{-1}) for D_2O. The parameter c was found equal to $c = 0.35$ and $c = 0.50$ for H_2O and D_2O, respectively, with an estimated error of about 10%. Both the predissociation rates and the parameter c for H_2O are in good agreement with the values obtained in other studies,[5,6] whereas we find the value of c for D_2O approximately twice as large. The previous value certainly gives a too low heterogeneous predissociation rate especially for higher values of $\langle J_a'^2\rangle$ as already noticed by Docker *et al.*[7] These simulated spectra are shown below the observed ones in Figs. 8 and 9.

In the simulation of the REMPI spectra the influence of the ionization on the lifetime of the upper state is no longer negligible and has to be included in the term β. The value of β depends on the power density in the region of ion production, which implies that it depends on details of the experimental setup. For the fit we use

$$\Delta\nu = (1+c\langle J_a'^2\rangle+\beta)\cdot\Delta\nu_0,$$
$$h_{\text{ion}}(:)h_0/(1+c\langle J_a'^2\rangle+\beta)^2. \tag{3}$$

With the same values of $\Delta\nu_0$ and c the REMPI spectra could be fairly well simulated with $\beta = 1.5$ for H_2O and $\beta = 0.5$ for D_2O (Figs. 6 and 7). The fraction of the excited molecules that ionizes is equal to $\beta/(1+c\langle J_a'^2\rangle+\beta)$, which in our case reaches values up to 0.6 for H_2O and to 0.3 for D_2O. Obviously the last ionization step is not completely saturated, due to the competing predissociation. This can explain the near cubic power dependence of the ion yield for D_2O. Furthermore, the difference in the value of β between H_2O and D_2O is consistent with the different power dependence of the yield for H_2O and D_2O, as seen in Fig. 3.

The excited photofragments are formed via heterogeneous predissociation into the dissociative $\tilde{B}\,^1A_1$ state. In the simulation of the OH/OD ($A \rightarrow X$) excitation spectra we used the following formulas, analogous to Hodgson *et al.*[5]:

$$\Delta\nu = (1+c\langle J_a'^2\rangle)\cdot\Delta\nu_0,$$
$$h(:)h_0\langle J_a'^2\rangle e^{-0.1\langle J_a'^2\rangle}/(1+c\langle J_a'^2\rangle)^2. \tag{4}$$

The exponential factor takes branching out of the $\tilde{B}\,^1A_1$ state into a "dark channel" into account.[5] Using the values obtained for $\Delta\nu_0$ and c the simulated spectra are in good agreement with the observed spectra both in line positions and in relative intensities, as can be seen in Figs. 4 and 5.

IV. CONCLUSIONS

The (2 + 1)-REMPI spectra of H_2O and D_2O are presented and almost quantitatively interpreted. It is shown that direct three photon ionizaton of H_2O and D_2O with a tunable excimer laser can be used for sensitive quantum state specific detection of these molecules. The important rotational two-photon transitions involved are tabulated. The very high ion yield allows a simple detection method. If ion

counting is applied state selective detection must be possible at very low partial pressures. At high gas pressures the molecular fluorescence in the blue can also be used for state selective detection, although the overall detection efficiency is approximately a factor 10^5–10^6 lower.

A difference is found in the ionization rate between H_2O and D_2O. Both from the power dependence of the ion signal and from the simulation of the observed $(2+1)$-REMPI spectra it looks as if H_2O is more easily ionized than D_2O. This is quite unexpected as the predissociation of the excited $\tilde{C}\,^1B_1$ state is about a factor of 2 stronger for H_2O than for D_2O.

Especially in the case of H_2O, where the $(2+1)$-REMPI spectrum consists of several clearly separated rotational transitions from low rotational levels in the ground state, conveniently situated near the middle of the KrF gain profile, $(2+1)$-REMPI must be possible in a supersonic molecular beam. Work is in progress to realize this.

ACKNOWLEDGMENTS

We are grateful to Professor R. N. Dixon for sending us the calculated two-photon line strengths, and to Professor D. H. Parker and Professor A. Dymanus for helpful discussions. Part of this work has been supported by the Stichting voor Fundamenteel Onderzoek der Materie (FOM) and has been made possible by financial support from the Nederlandse Organisatie voor Zuiver Wetenschappelijk Onderzoek (ZWO) and from the Deutsche Forschungsgemeinschaft.

[1] T. Carrington, J. Chem. Phys. **41**, 2012 (1964).
[2] H. Okabe, J. Chem. Phys. **72**, 6642 (1980).
[3] J. P. Simons, A. J. Smith, and R. N. Dixon, J. Chem. Soc. Faraday Trans. 2 **80**, 1489 (1984).
[4] C. Fotakis, C. B. McKendrick, and R. J. Donovan, Chem. Phys. Lett. **80**, 598 (1981).
[5] A. Hodgson, J. P. Simons, M. N. R. Ashfold, J. M. Bayley, and R. N. Dixon, Mol. Phys. **54**, 351 (1985).
[6] M. N. R. Ashfold, J. M. Bayley, and R. N. Dixon, Chem. Phys. **84**, 35 (1984).
[7] M. P. Docker, A. Hodgson, and J. P. Simons, Mol. Phys. **57**, 129 (1986).
[8] E. W. Rothe, G. S. Ondrey, and P. Andresen, Opt. Commun. **58**, 113 (1986).
[9] R. N. Dixon (private communication).
[10] G. W. Loge and J. R. Wiesenfeld, J. Chem. Phys. **75**, 2795 (1981).
[11] (a) J. W. C. Johns, Can. J. Phys. **41**, 209 (1963); (b) **49**, 944 (1971).
[12] C. Carlone and F. W. Dalby, Can. J. Phys. **47**, 1945 (1969).
[13] D. R. Crosley and R. K. Lengel, J. Quant. Spectrosc. Radiat. Transfer **15**, 579 (1975).
[14] P. E. Rousse and R. Engleman, Jr., Quant. Spectrosc. Radiat. Transfer **13**, 1503 (1973).
[15] D. S. Zakheim and P. M. Johnson, Chem. Phys. **46**, 263 (1980).
[16] S. Tsurubuchi, Chem. Phys. **10**, 335 (1975).
[17] J. A. Coxon, J. Mol. Spectrosc. **58**, 1 (1975).